Journal of Structural Geology, Vol. 6, No. 5, pp. 543 to 562, 1984
Printed in Great Britain

0191-8141/84 $03.00 + 0.00
© 1984 Pergamon Press Ltd.

Strain analysis and strain path modelling in the Loch Tollie gneisses, Gairloch, NW Scotland

N. E. ODLING*

Grant Institute of Geology, University of Edinburgh, West Mains Road, Edinburgh, EH9 3JW, U.K.

(*Received* 10 *February* 1983; *accepted in revised form* 8 *November* 1983)

Abstract—A quantitative structural analysis is presented for the Loch Tollie gneisses of the Lewisian complex outcropping at Gairloch. The gneisses and the dykes they contain are folded into a large antiformal structure known as the Tollie Antiform. Quartz aggregates in quartzo-feldspathic gneisses have been used as finite strain markers in eleven specimens across the antiform. Two models, using rotational strain (simple shear) and irrotational strain (pure shear), are used to reconstruct the strain path. Results show that only the rotational strain model satisfies the strain data and the field evidence, and indicates a steeply northeast (75°) dipping shear plane and moderately northwest (55°) plunging shear direction, with a southwest-side-down sense of shear. A strain profile is constructed for the Tollie gneisses using the model and the attitude of gneissose layering. This shows increasing shear strain to the southwest to a maximum gamma value of approximately 8. The strain profile indicates a horizontal dextral displacement of 4.7 km and a vertical displacement of 6.8 km for the Tollie gneisses. The Tollie Antiform thus lies on the northeast margin of a large-scale shear zone, the main zone of deformation of which can be traced southwestwards some 4 km. Such a shear zone presents a major tectonic boundary within the Lewisian of northwest Scotland.

INTRODUCTION

THE LOCH TOLLIE Gneisses comprise the northeast portion of the Lewisian gneiss complex outcropping at Gairloch, being bordered to the north by the Loch Maree Fault and to the south by the Gairloch schist belt (Fig. 1). The area was first mapped by Clough and Gunn (Peach *et al.* 1907, chapter 2) and more recently by Park (1969). Park gives a detailed structural analysis based on minor structures, inferring five phases of deformation.

The rocks are hornblende, biotite and quartzo-feldspathic layered gneisses with subparallel amphibolitized dykes, all in the amphibolite grade of metamorphism (Park 1969). The gneissose layering and dykes are folded into an antiform known as the Tollie Antiform, with a moderately northeast (50°) dipping northeast limb, subvertical southwest limb and gently to moderately southeast (10–60°) plunging hinge within the area shown in Fig. 2.

Lineations, consisting of elongation of quartz aggregates in the gneisses and mineral lineations in the dykes, plunge moderately southeast in the northeast limb, becoming subhorizontal in the crest of the antiform, and ranging from gentle southeast to moderate northwest in the southwest limb (Fig. 2). A rodding lineation, consisting of small-scale fold hinges in the quartz aggregates, is also developed in the gneisses of the southwest limb. These range from gently southeast plunging near the crest of the fold, through horizontal to moderately plunging northwest, in a southwesterly direction across the fold limb. There is a change in style and inter-limb angle of folds across the antiform. In the northeast limb, folds have interlimb angles of 60 ± 20°, with similar to parallel styles. These folds become progressively more open towards the crest of the fold. In the crest, folds have large interlimb angles, around 130°, and are strongly disharmonic with styles approximating to parallel. Entering the southwest limb, folds become tighter with interlimb angles of around 50° or less, and the style becomes similar with sharp hinges being common. Towards the southwest the scale of gneissose layering becomes progressively finer and folds become isoclinal and strongly attenuated.

This variation in fold geometry is accompanied by a general decrease in grain size of both gneisses and dykes southwestwards through the steep southwest limb of the antiform. This, with the variation in fold style and inter-limb angle, and scale of gneissose layering, all indicate a general increase in the intensity of deformation to the southwest.

Shape fabrics shown by the quartz aggregates in the gneisses and mineral fabrics shown by hornblende and biotite in the dykes (Fig. 2) range from near LS in the northeast limb, through markedly L in the crest to a sequence of LS, S and LS southwestwards across the southwest limb.

The style of the antiform varies along strike with a broad flat crest in the northwest and becoming more angular to the southeast where the crest of the fold is much narrower. The lens-shaped outcrop of strongly linear fabrics (Fig. 2), includes the broad crest of the antiform and the northern part of the northeast limb. The area investigated in this study is that part of the antiform where the fold is broadest and the greatest

* Present address: Precambrian Research Unit, University of Cape Town, Private Bag, Rondebosch, 7700, Cape Town, South Africa.

Notation: X, Y, Z: Maximum, intermediate and minimum axes of the strain ellipsoid.
Axial ratios are defined as follows: $a = X/Y$, $b = Y/Z$ and $K = (a - 1)/(b - 1)$.
Description of strain ellipsoid and fabric types: L, prolate ellipsoids and strongly linear fabrics ($K \gg 1$); S, oblate ellipsoids and strongly planar fabrics ($K \ll 1$) and LS, plane strain and fabrics in which linear and planar elements are approximately equally strong ($K = 1$).

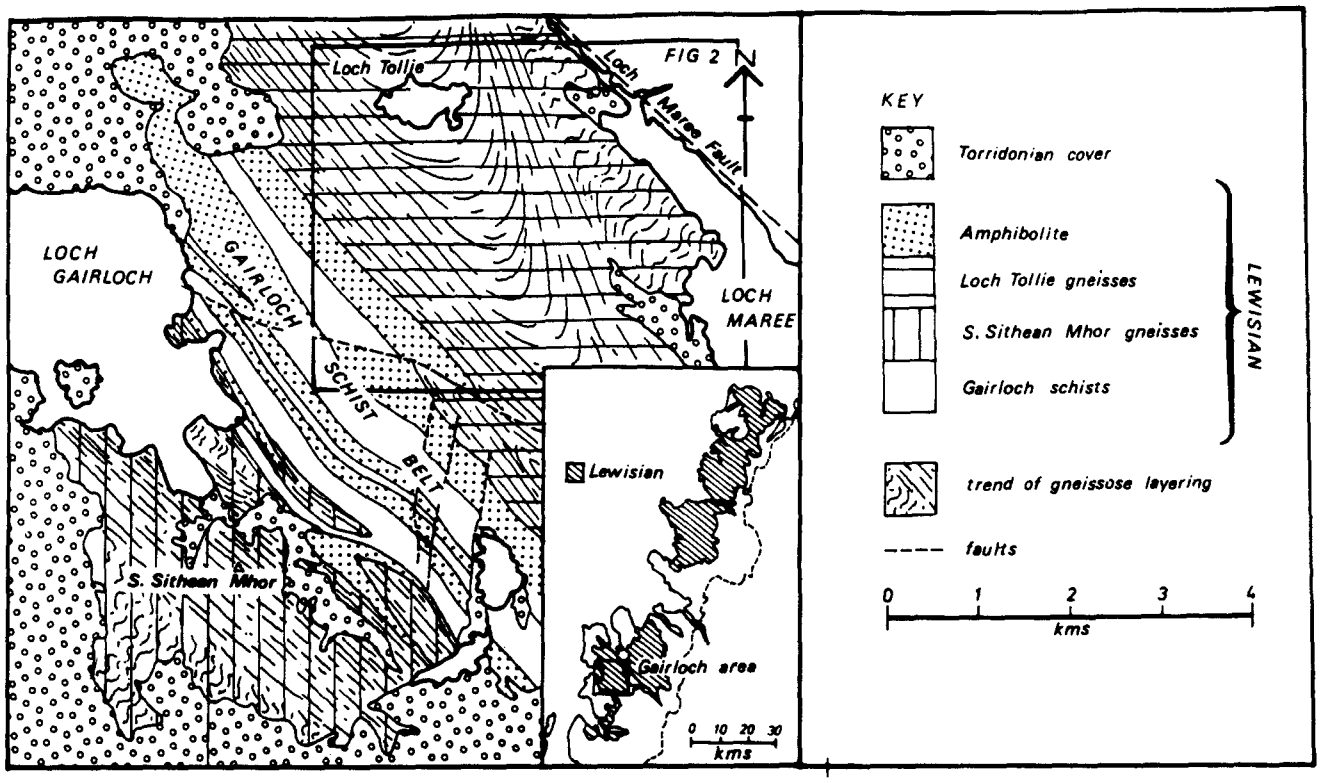

Fig. 1. Geological map of the Gairloch area with the location of Fig. 2 outlined.

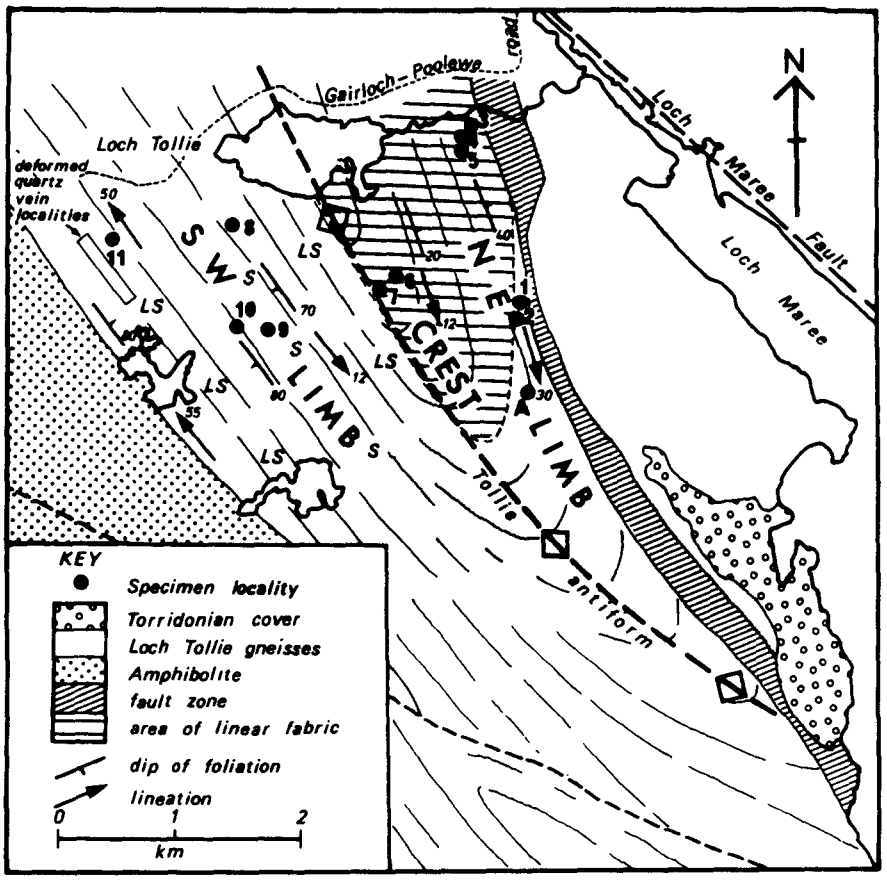

Fig. 2. Structural geology of the Loch Tollie area showing distribution of fabric types and location of specimens 1 to 11 and A (black dots).

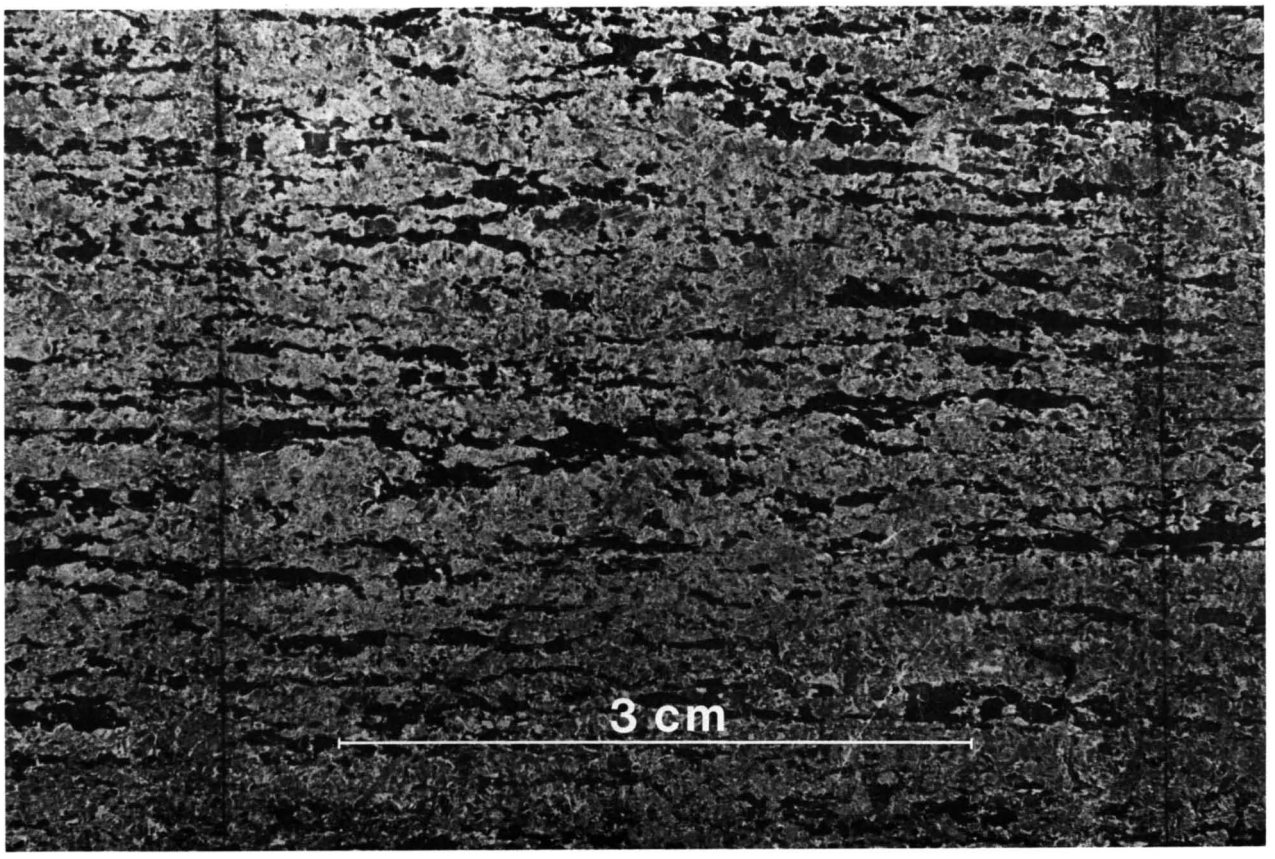

Fig. 3. Photograph of an acetate peel made from an etched and stained slab of quartzo-feldspathic gneiss (specimen 1). Dark areas are quartz, lighter areas are plagioclase and K-feldspar.

variety of fabrics is found, that is, the area within 3 km southeast of the Gairloch–Poolewe Road (Fig. 2). The aim of the present study is to produce a quantitative structural analysis of the area based on strain analysis and strain path modelling.

STRAIN ANALYSIS

Strain markers and procedure

Quartz particles in quartzo-feldspathic gneiss are used as strain markers. These particles are highly irregular in shape (Fig. 3), and range in size from approximately 1 mm to 1 cm, forming 25–35% of the rock. Results from the average volume of particles per specimen, calculated in the course of strain analysis, show no correlation between size of quartz aggregate and their deformation state, suggesting that the particles have suffered no major volume loss or gain during deformation. The effect due to the competence or viscosity difference between quartz and feldspar has also been investigated (Odling 1980, chapter 4). Finite strain as recorded by the quartz particles was found to overestimate the bulk strain by approximately 10%. This is due to the quartz particles being of lower 'viscosity' or competency than feldspar, so that the quartz particles deform more readily than the feldspar matrix and thus the rock as a whole. To minimize the effects of the presence of other minerals, only quartzo-feldspathic gneisses with less than approximately 2% biotite or hornblende were used. For each specimen, three randomly oriented, mutually perpendicular faces were cut. The faces were etched with 40% hydrofluoric acid and stained with sodium cobaltinitrite (Bailey & Stevens 1960). After treatment the quartz particles remained clear while the feldspars were stained yellow (K-feldspar) or white (plagioclase). Acetate peels were made of the etched slabs and enlarged projections of the peels used to select and trace thirty-three quartz particles per peel using a grid system to avoid bias. From an investigation in two dimensions (Odling 1980, pp. 47–49), it was found that two independent samples of thirty-three grains of one face of specimen 1 gave the axial ratio of the average ellipse to within 0.1 and the orientation of the long axis to within 0.6°. The diameters of each quartz particle were measured in 6–8 common directions and the diameters averaged for each direction (Fig. 4). Average diameter lengths for each face were adjusted by a constant factor so that the misfits were approximately equal on all three face intersections. The average diameters were then used to calculate the ellipsoid approximating most closely to the average particle shape using the method outlined by Hext (1963).

In the method of Hext (1963), the three-dimensional ellipsoid is calculated directly from the average diameter lengths and their orientations. The calculation is executed by the unpublished computer programme 'PATEN', written by R. F. Cheeney, Department of Geology, Edinburgh University. The programme output

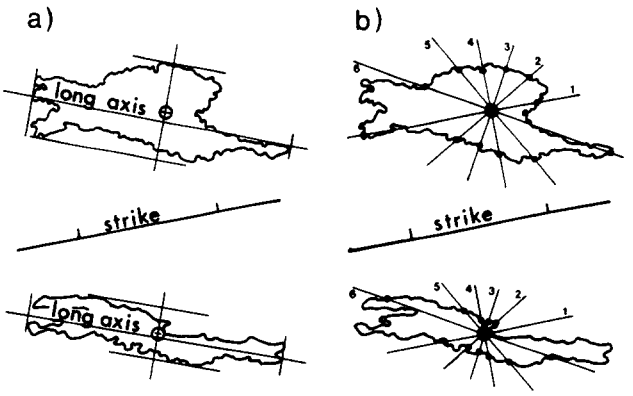

Fig. 4. (a) Location of the centres of two particles traced from Fig. 3. The long axis is located by eye and its maximum length halved. The maximum breadth perpendicular to the long axis is drawn at this point and the particle's centre is located at the mid-point of this breadth (circles). (b) Six equally spaced common diameters passing through the particle centres are measured for each particle and the measurements for each of the diameter directions 1 to 6 are summed. This average particle shape approximates to the finite strain ellipse.

gives the lengths of the principal axes of the best fit ellipsoid and their orientations with 95% confidence limits and cones. The best fit ellipse is equivalent to the strain ellipsoid if the particle long axes are initially randomly oriented (Shimamoto & Ikeda 1976). No quartzo-feldspathic gneisses showing isotropic fabric occur in the Tollie area so a specimen from the S. Sithean Mhor area to the south of the Gairloch schist belt, where near isotropic fabrics occur, was used to test the condition of initial random orientation of quartz aggregates. On application of the above method, this specimen gave an average ellipsoid with axial ratios X/Y of 1.57 and Y/Z of 1.02, showing very low strain compared to the deformed gneisses of the Tollie Antiform. Though the Loch Tollie and South Sithean Mhor gneisses are separated by the Gairloch schist belt, and are therefore unlikely to be equivalent, similarities of the two lithologies such as their layered nature and the presence in both of amphibolite, hornblendite and other pods, suggest that the Tollie gneisses, prior to deformation, also satisfied the condition of initial random orientation of quartz aggregates.

The Rf/ϕ method (Dunnet & Siddans 1971) was also used to test the condition of initial random fabric on nine two-dimensional sections from the specimens used for three-dimensional analysis. In this method, the axial ratio (Rf) is plotted against the orientation of the long axis (ϕ) and the symmetry of the resultant plot gives information on the fabric prior to deformation. The plots for each of the above nine specimens were divided into four quadrants by the 50% data curve and the mean ϕ value (Dunnet & Siddans 1971) and on application of the chi-square test, the difference in number of points of each quadrant was found to be insignificant at the 99% confidence level for all nine specimens. The distribution of points on the Rf/ϕ plots with respect to 'onion curves' of Dunnet (1969) (curves of equal initial ellipse axial ratio) show a range of initial axial ratios from 1.0 to 3.0. A lack of concentration relating to any single 'onion' curve indicates a random distribution of initial ratios

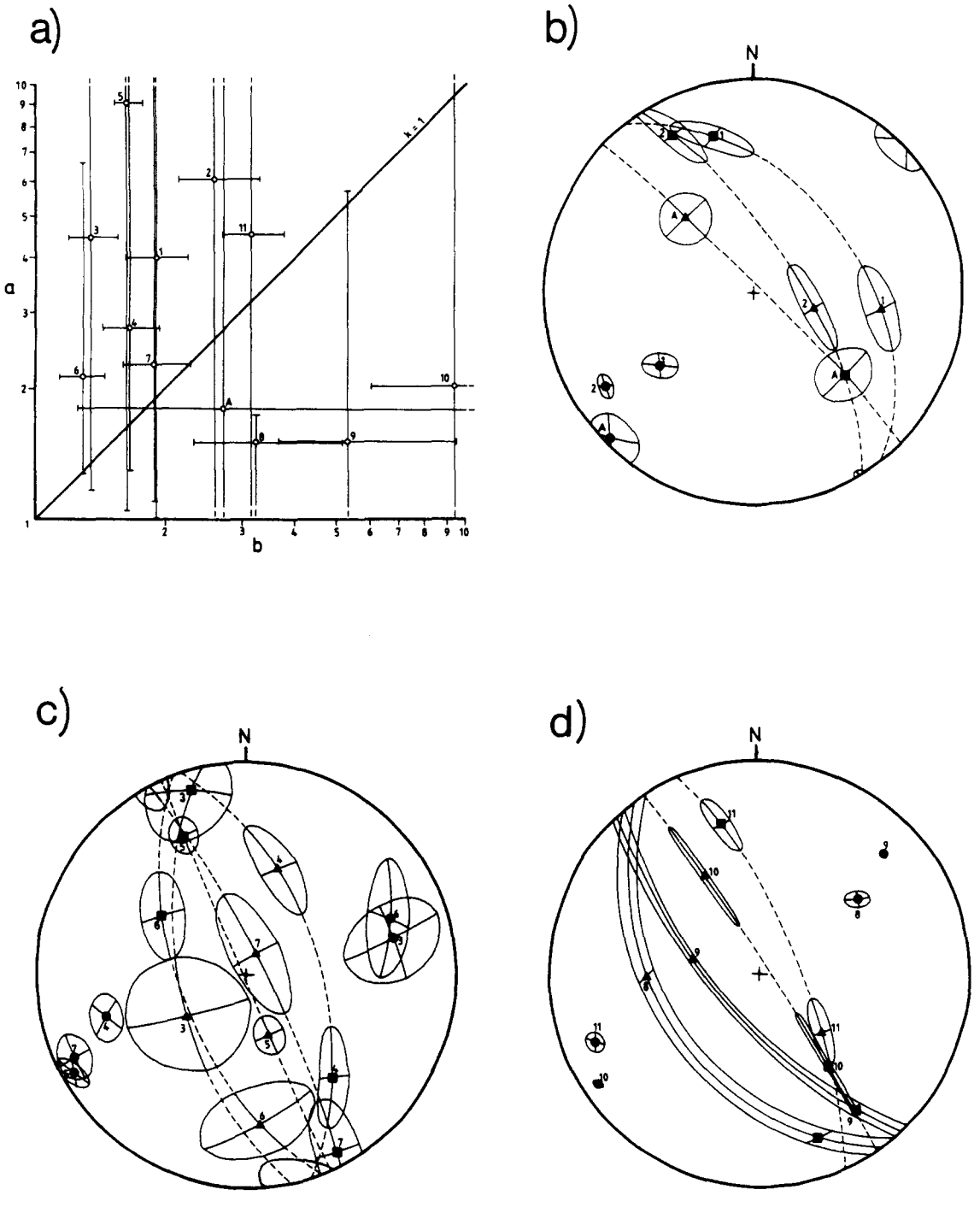

Fig. 5. Results of finite strain analysis. (a) Ratio a (X/Y) vs b (Y/Z) for principal strain axes with 95% confidence limits, plotted on $\log_{10}$ deformation plot. (b), (c) and (d) Orientations of principal strain axes for (b) the northeast limb, (c) the crest of the antiform and (d) the southwest limb, with 95% confidence cones. Squares, maxima (X); triangles, intermediate axes (Y); circles, minima (Z).

within this range. Such symmetry implies an initially random fabric and thus the best fit ellipsoid is equivalent to the strain ellipsoid.

Twelve rocks collected from a northeast–southwest profile across the Tollie Antiform (Fig. 2) have been analysed for strain by the above method.

Results

The results of the three-dimensional strain analysis are plotted in Fig. 5. Figure 5(a) shows the ratios 'a' (X/Y) and 'b' (Y/Z) of the principal axes plotted on a logarithmic deformation plot with 95% confidence limits. Figures 5(b–d) show the orientations of the principal axes with 95% confidence cones plotted on a lower hemisphere Lambert equal-area net.

Confidence intervals on the ratios a and b, calculated using the equation given by Topping (1958, p. 82), were found to be large, the upper confidence limit for a in many cases lying outside the domain of real numbers. This is possible as the theory of Hext (1963) fits the data to a quadratic surface, of which an ellipsoid is only one type. Where the quadratic surface is not an ellipsoid the upper confidence limit on the maximum axis (and, therefore, on a) is not available. The confidence intervals would seem to imply poor precision of the data. How-

ever, several considerations indicate that the data is more reliable than such confidence intervals would suggest.

(1) The ellipsoid type indicated by a and b ratios correlates with the confidence interval pattern on orientations, i.e. in ellipsoids close to S type ($X = Y \gg Z$ i.e. $b \gg a$) confidence cones show that X and Y directions are indistinguishable (specimens 8 and 9, Figs. 5a & d). Also where ellipsoids are close to L in type ($a \gg b$), the orientation of X is precisely defined (specimens 5, 3 and 6, Figs. 5a & c).

(2) The strain data agrees with qualitative estimation of fabric type in the field as indicated by shape and mineral fabrics. The shape fabrics are formed by quartz aggregates in the gneisses and feldspar aggregates in the dykes, and mineral fabrics by alignment of biotite and hornblende in the gneisses and hornblende in the dykes. These fabrics show a sequence from near LS to L in the northeast limb, to strongly L in the flat belt and a progression southwestwards from LS to S and back to LS within the southwest limb. This is in agreement with the strain analysis results, with specimens 1 and 2 showing LS strains with an L component and specimens 3 and 5 showing strong L strains from the northeast limb; specimens 6 and 7 from the crest of the antiform showing LS strains with an L component; specimens 8, 9 and 10 from the southwest limb showing progressively more intense S strains; and specimen 11 from the extreme southwest of the southwest limb showing LS strain. Only specimen 4 does not fit this pattern showing a fabric closer to LS than specimens 3 and 5 and having a southeast plunging maximum. This specimen shows a similar fabric to that found 2 km to the south of the traverse represented by specimen A and probably represents an isolated occurrence of this fabric type.

The maxima for specimens 1–7 plunge either gently northwest or southeast. Lineations measured in the field for the northeast limb and flat belt plunge gently southeast. In this area, because shape fabrics are linear in nature the gneissose layering controls weathering and exposed surfaces are often parallel to this layering which dips east to southeast. These measured lineations are therefore intersection linetions between quartz shape fabrics and gneissose layering and the quartz shape fabric lineations themselves plunge gently northwest.

The X–Y planes for specimens 1–5 dip steeply northeast or southwest, though such foliation is hard to distinguish in the field due to the strong linear nature of the shape and mineral fabrics. X–Y planes for specimens 6 and 7, at the crest of the antiform dip vertically to steeply southwest in agreement with the foliation observed in the gneisses.

The maxima for specimens 8–10 plunge gently to moderately southeast with X–Y planes dipping vertically to moderately southwest. A strong lineation is developed in the southwest limb which plunges gently southeast becoming horizontal to northwest plunging, southwestwards across the limb, as recorded by Park (1969). However, this lineation was found to be composed of micro-fold hinges and is thus not necessarily parallel to shape fabric lineations or strain ellipsoid maxima. The shape and mineral fabrics in this area were found to be strongly planar and the associated lineation poorly developed or absent. However, the foliation here is well defined and coincides with the strain data X–Y planes, specimens 8–10, becoming progressively steeper southwestwards. The strong S strains shown by the results for specimens 8–10 are supported by 'chocolate tablet' structure in the dykes found in this area where boudinage of dykes has occurred in all directions within the plane of the foliation to which the dykes are subparallel. This implies extension in all directions within the plane of the foliation and thus a strain of S type in agreement with the strain analysis.

Specimen 11 from the southwestern edge of the southwest limb shows close to LS strains with a moderately northwest plunging maximum. In this area the fabric types were observed to be LS with shape fabric and mineral lineations plunging northwest in agreement with the maximum of the strain ellipsoid. The X–Y plane of specimen 11 dips steeply northeast, in agreement with the gneissose foliation orientation in this area.

Thus the type and orientation of the strain ellipsoid correlates with the lineations and foliations formed by shape and mineral fabrics of gneisses and dykes as observed in the field. Extra supporting evidence for the S strains in the southwest limb is given by the boudinage of dykes resulting in 'chocolate-tablet' structure. Thus, confidence limits on the lengths of principal axes are thought to give a misleading view of the precision of the data and are, therefore, omitted on succeeding diagrams. However, better confidence cones on axis orientations than confidence limits on the ratios a and b, indicate that more emphasis should be placed on the orientation of axes in the interpretation of the data.

MODELLING THE STRAIN PATH

Several aspects of the field evidence indicate a general increase in deformation to the southwest. These include:

(1) A decrease in width of gneissose layering and dykes from the northeast limb and flat belt to the southwest limb. In the southwest limb, dykes and gneissose layering become strongly attenuated and the thickness of gneissose layering is reduced from the order of tens of cm to cm or fractions of a cm.

(2) The progressive southwestwards decrease in fold interlimb angle from the flat belt through the southwest limb. In the flat belt, folds are very open often with interlimb angles of 150° or more, which at the crest of the antiform become tighter, around 45°. In the southwest limb, interlimb angles decrease until the style is isoclinal and in the extreme southwest all folds are strongly attenuated, to such an extent that they are often difficult to distinguish in the field.

(3) A general decrease in grain size of all minerals towards the southwest, most noticeable in the southwest limb. In the gneisses, quartz aggregates become recrystallized and the feldspar matrix becomes finer grained.

In the dykes, the coarse hornblende laths, approximately 5 mm long, and feldspar aggregates found in the northeast limb and flat belt, are recrystallized in the southwest limb to a fine grain size of 1 mm or less, while feldspar aggregates are smeared out and finally dispersed. In the quartzo-feldspathic gneisses, even the finest grained examples show a feldspar matrix approaching polygonal texture while the quartz aggregates show division into new smaller grains with undulose extinction. These features indicate that the textures approach a stable configuration. If these textures are syntectonic in origin and post-tectonic recrystallization is minimal, they imply dynamic recrystallization as the mechanism of grain size reduction and thus an increase in stress and strain rate to the southwest, during deformation.

(4) A marked increase in the attenuation of quartz aggregates and hornblendite and amphibolite pods within the gneisses southwestwards from the northeast limb. Pods and quartz aggregates show increased elongation in the flat belt and, in the southwest limb, boudinage of pods and dykes is common often with nodes of quartz between boudins.

The features listed above, all indicate a general increase in deformation to the southwest with a sharp increase occurring in the southwest limb. Thus the rocks of the extreme northeast are the least deformed. For the purposes of the strain model, therefore, these rocks are regarded as representing an initial fabric upon which deformation has acted to produce the fabrics to the southwest. The theoretical models investigated are of two types:

(1) rotational strain model—deformation by simple shear where the Tollie Antiform is formed as a consequence of the deformation and

(2) irrotational strain model—deformation by pure shear where formation of the Tollie Antiform must precede the deformation.

Both models were constructed using an unpublished computer programme called 'SUST' written by D. Sanderson (Belfast). The programme converts the initial fabric (an ellipsoid) and the finite strain to 3×3 matrices and the resulting ellipsoid is computed by matrix multiplication. Thus it is possible to compute the result of any finite strain (pure shear, simple shear or a combination of the two) superimposed on any initial ellipsoid.

Rotational Strain Model

The model was constructed using progressive amounts of simple shear superimposed on the fabric of the northeast limb. The variables in the model are initial fabric, shear plane orientation, shear direction and sense and increments of shear. Field evidence was used to fix the initial fabric, shear plane orientation and shear sense.

(1) *Initial fabric.* As has already been mentioned, the rocks of the northeast limb are the least deformed of the area, and thus for the model, specimen 1, which has a dominantly linear fabric with minor planar element and a gently north plunging maximum axis (Fig. 5), is used as an example of the initial fabric.

(2) *Shear plane orientation.* The orientation of foliation in the most highly deformed rocks to the southwest, dip 75° direction 040°, is used. This orientation of foliation is common to all the rocks in the centre of the Lewisian inlier, from the southwest limb of the Tollie Antiform to the South Sithean Mhor gneisses, see Fig. 1. The foliation defined by quartz shape fabrics in the gneisses and mineral alignment in the schists will, in theory, never reach the orientation of the shear plane. However, the schists show evidence of extreme deformation, i.e. blastomylonitic textures and very fine grain size, streaked out feldspar aggregates in amphibolites, and extreme quartz shape fabrics in gneiss layers included in the schists (Odling 1980, chapter 8). Under these conditions the foliation will lie within a few degrees, and thus give a close approximation to, the shear plane orientation.

(3) *The shear direction and sense.* The Tollie Antiform itself implies a southwest-side-down sense, i.e. negative with respect to right handed orthogonal axes, where X points north, Y east and Z down. Lineation orientations in the extreme southwest of the antiform suggest a northwest plunging shear direction and to test this hypothesis a range of eight shear directions within the shear plane, all of negative sense, are used in the model (Table 1).

Table 1. Strain model shear directions (rotational strain model) and orientation of maxima (irrotational strain model) for models 1 to 8

Model	Plunge and direction of plunge (in degrees)
1	11313
2	38 322
3	55 333
4	71 001
5	73 069
6	52 110
7	29 121
8	14 125

(4) *Increments of shear.* Since in progressive simple shear deformation finite strain values and principal axes orientations tend to change most rapidly in the initial stages, the increments of shear (γ) are chosen as: 0.2, 0.5, 1.0, 1.5, 2.0, 2.5, 3.0, 4.0, 6.0 and 8.0.

Results

The results of modelling the eight shear directions are plotted in Figs. 6(a–c). Figure 6(b) shows that only northwest plunging shear directions (models 1–4) produce ultimately northwest plunging maxima and Fig. 6(a) shows that of these only models 3 and 4 produce L ($K > 1$) fabrics, followed by S ($K < 1$) and LS ($K = 1$) fabrics. All southeast plunging directions (models 5–8) produce only southeast plunging maxima and do not produce markedly linear fabrics.

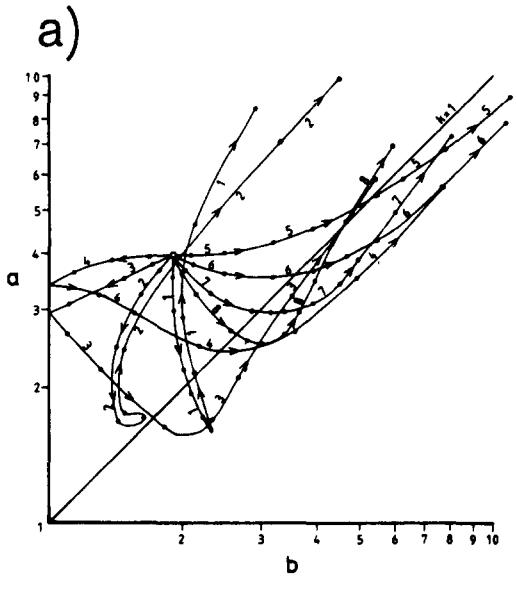

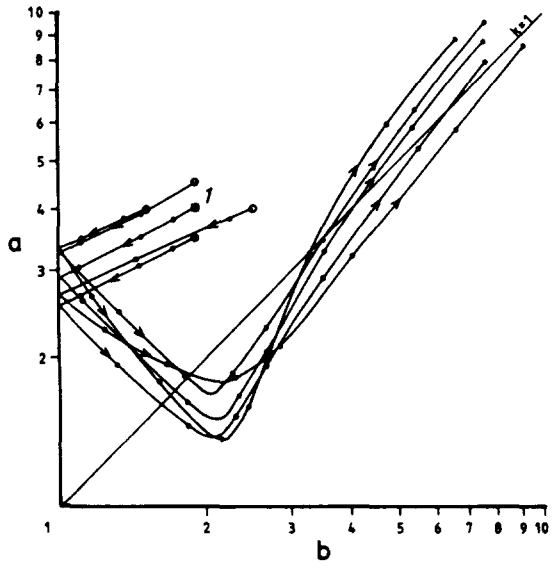

Fig. 7. Rotational strain model: shear direction 3 (55°333°), showing the effect of variation in ratios a and b on the strain path. Open square, initial fabric, specimen 1, northeast limb; open circles, variation on ratios a and b of initial fabric of 0.5. Values of shear strain as for Fig. 6.

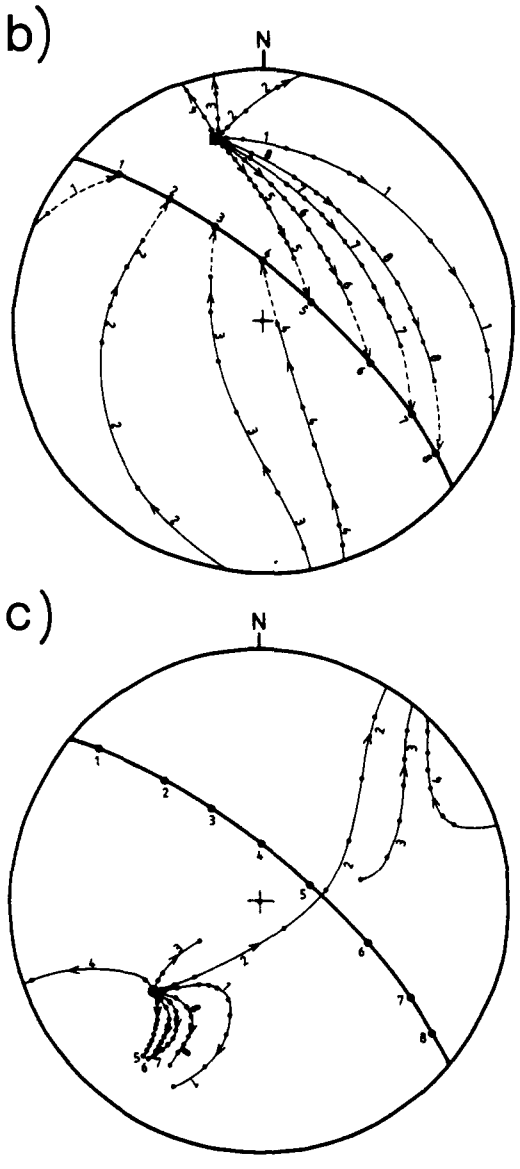

Fig. 6. Rotational strain model (simple shear). The shear plane orientation is 75°040° and the shear directions 1–8 are listed in Table 1. The strain paths are constructed using the sequence of shear strain values (γ) 0.2, 0.5, 1.0, 1.5, 2.0, 2.5, 3.0, 4.0, 6.0 and 8.0 (small dots). The initial fabric (square, maximum; circle, minimum) is specimen 1 from the northeast limb. (a) Strain path of principal axes ratios a (X/Y) vs b (Y/Z) for shear directions 1–8. (b) and (c) Strain path of maximum (X) and minimum (Z) orientations, respectively, for shear directions 1–8.

Of models 3 and 4, model 3 (shear direction 55°, 333°) produces the best fit to foliation (X–Y) plane orientations and the fabric variation giving the sequence from L ($K > 1$) through LS ($K = 1$) to S ($K < 1$), finally returning to LS ($K = 1$) fabrics. This is in agreement with the field evidence for a moderately northwest plunging shear direction. Model 3 has been tested for stability with respect to ratios a and b (Fig. 7), which shows that variations in a and b up to 0.5 have little effect on the strain path.

The results of the rotational strain model have been further tested by replacing the initial fabric of specimen 1 by the other specimens occurring in the northeast limb, i.e. specimens 2–5. The model was applied to each of these specimens using the best fitting shear direction (Fig. 6) found for specimen 1, model 3, and the shear directions on either side, models 2 and 4. The resulting strain paths are plotted in Fig. 8.

Specimens 2, 3 and 5 have initially gently northwest plunging maxima and on shearing by models 2–4 follow the same kind of path as specimen 1, passing through the horizontal and rotating further through southerly plunges to become moderately plunging northwest. The deformation paths of minima of these specimens also show broadly similar patterns to specimen 1. Specimens 3 and 5 do not show a path towards more intensely linear fabrics, but both these specimens have already strong L fabrics and the rest of the deformation path follows that of specimen 1, crossing the $K = 1$ line into the flattening field and finally returning to the $K = 1$ line. Specimen 5 shows the best development of S strains with paths for models 2–4 that pass close to the location of specimens 8–10, whereas specimen 2 shows the least development of S strains, crossing briefly into the flattening field, though this specimen does show some increase in the intensity of L strains before the path crosses the $K = 1$ line.

Specimen 4 is the only one that does not show a return

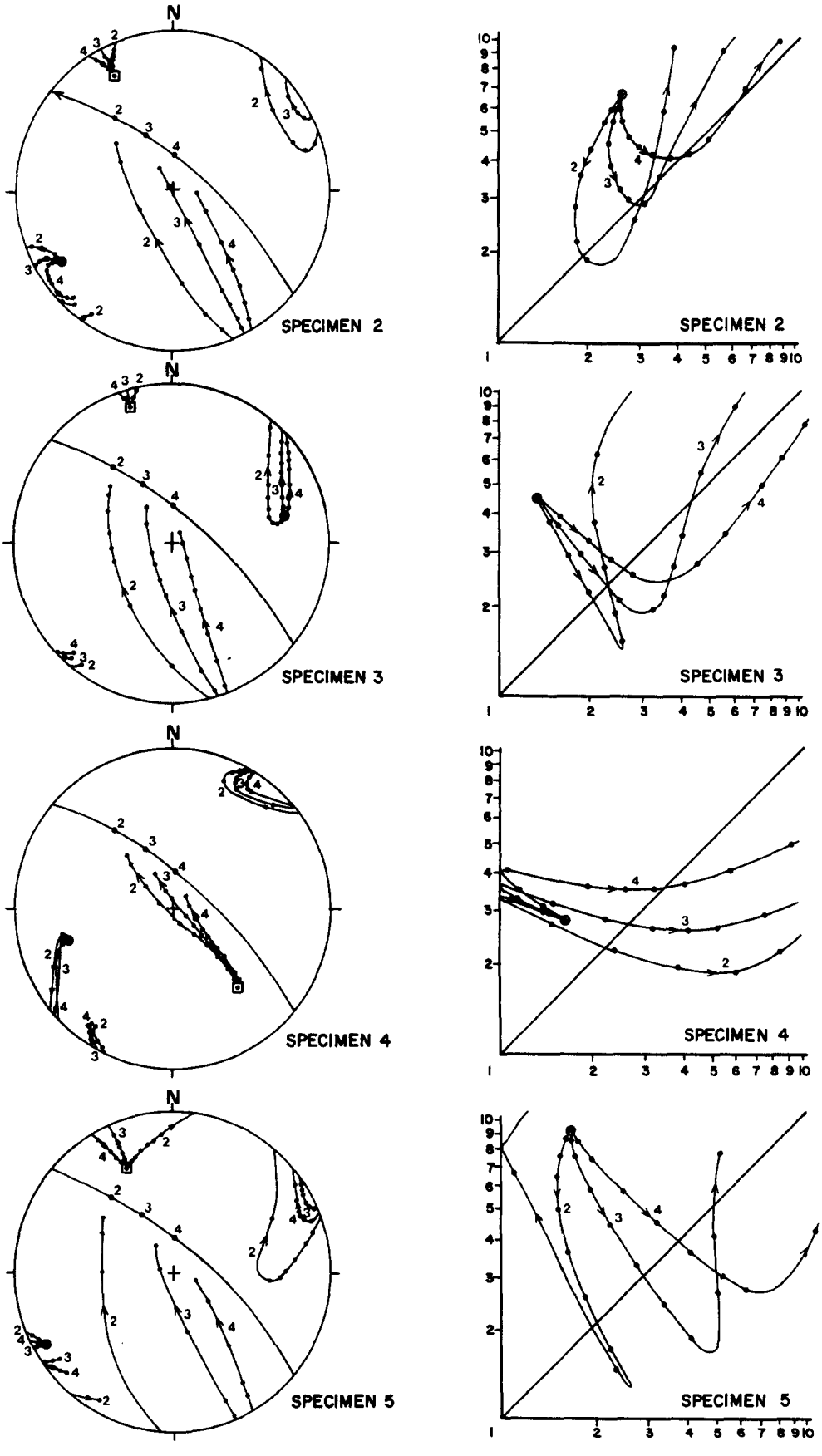

Fig. 8. Rotational strain model: results of models 2–4 using specimens 2–5, respectively as initial fabric. Squares, maxima (X); circles, minima (Z). Values of shear strain as for Fig. 6.

to the $K = 1$ line after passing into the flattening field. This specimen is anomalous in that it shows a moderately southeast plunging maximum and closer to LS fabric in contrast to specimens 1, 2, 3 and 5 which have gently north plunging maxima and strong L fabric types. As already mentioned, specimen 4 is probably related to the southeast plunging fabrics found 2 km to the south and represented by specimen A. The significance of these fabric types is discussed later in the paper.

For the remaining specimens, model 3 provides the best fit to the strain data for 1, 3 and 5 whereas model 2 shows the best fit for specimen 2. Overall, therefore, model 3 provides the best fit to the strain data. The deformation paths of maxima and minima show very similar paths, indicating that the variation in axial ratios has little effect on the paths of the principal axes. The logarithmic deformation plots of Fig. 8 show a variety of paths but all, except specimen 4, show a similar overall pattern. The paths of specimen 5, models 2–4 show strongly flattened fabrics covering the plots of specimens 8–10. Model 3 for specimens 2, 3 and 5, and model 4 for specimen 2 recross the $K = 1$ line close to the location of specimen 11. Thus a variation in initial fabric produces similar styles of strain paths, and a variation in initial fabric as illustrated by specimens 1, 2, 3 and 5, in part explains the wide variation in a and b values of the strain results.

Irrotational strain model

In this model, the Tollie Antiform represents a pre-existing fold which has been progressively deformed to the southwest by pure shear. The shape and orientation of the pre-existing fold is unknown, so the simplest case of a concentric, symmetrical fold, constructed by rotating the fabric of the northeast limb (the area of lowest deformation), specimen 1, about a gently southeast plunging hinge was used as a basis for the model (Fig. 9). The variables in the model are then initial fabric, orientation of the principal axes and increments of strain.

(1) *Initial fabric.* Progressive pure shear deformation was applied to two initial fabrics; the fabric of specimen 1 on (i) the crest and (ii) the southwest limb of the fold in Fig. 9.

(2) *Orientation of the principal axes of strain.* The foliation orientation in the most highly deformed part of the antiform (the southwest limb), 75°040°, was used as an estimate of the X–Y plane of strain and is, therefore, similar to the orientation of shear plane in the rotational model. A range of eight maximum strain orientations similar to the eight shear directions of the rotational model was used (Table 1), the strain maximum and X–Y plane orientations uniquely describing the orientation of pure shear strain.

(3) *Increments of strain.* These were set at $a = b = 1.1$, 1.25, 1.5, 2.0, 2.5, 3.0, 4.0, 6.0 and 8.0 to show the strain history.

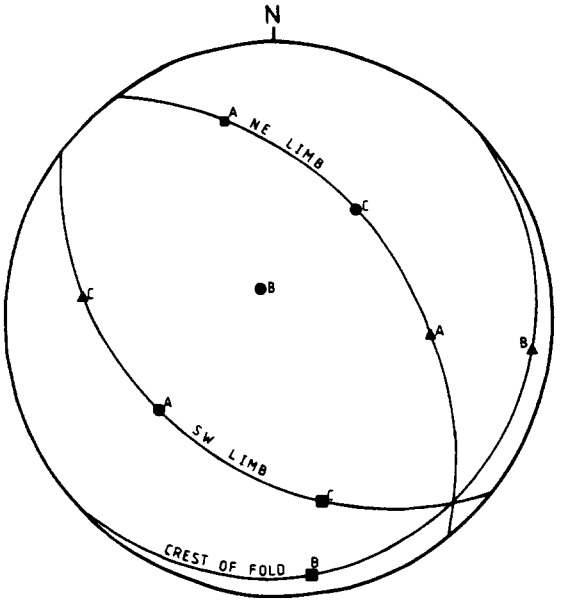

Fig. 9. Irrotational strain model: initial fabric, specimen 1 from the northeast limb (principal axes marked A) is concentrically folded about a hinge plunging gently southeast in agreement with the present plunge of the Tollie Antiform in the study area. The fold is the simplest starting fold for the model. Two initial orientations of the fabric of specimen 1 are used in the model corresponding to the crest of the fold (principal axes marked B) and the southwest limb (principal axes marked C). Squares, maxima (X); triangles, intermediate axes (Y), circles—minima (Z).

Results

The results of the model are shown in Figs. 10(a) and (b) for the crest of the fold and in Figs. 10(c) and (d) for the southwest limb of the fold.

(1) The crest of the fold: models 1–4, 7 and 8 produce stronger linear fabrics than those present in the northeast limb. Of these only models 1–4 give subhorizontal to gently northeast plunging maxima. These models give good linear fabrics after pure shear strains of $a = b = 1.5$–2.5, when maximum axes are subhorizontal, in agreement with the strain data.

(2) The southwest limb of the fold: only models 2–4 produce planar finite strains ($K < 1$), of which only models 2 and 3 produce northwest plunging maxima. None of the models produce LS ($K = 1$) fabrics after planar fabrics ($K < 1$) as observed in the strain data.

Repeating the irrotational model for specimens 2, 3 and 5 as representatives of the northeast limb gives strain path patterns similar to those for specimen 1 (Fig. 10). None of these initial fabrics were found to produce LS ($K = 1$) fabrics after S fabrics ($K < 1$).

After strains of $a = b = 8.0$, the principal axes of the resultant fabric are almost parallel to the principal axes of the irrotational strain ellipsoid. Under these conditions, Sanderson (1976) has shown that the strain path approaches a gradient of 1, parallel to the $K = 1$ line on a logarithmic deformation plot. Thus, under irrotational strain it is not possible for the strain paths in Fig. 10(c) to return to the $K = 1$ line after entering the S ($K < 1$) field, a condition which applies to any of the initial fabrics of the northeast limb (specimens 1–3 and 5). For specimens 1–3, model 3 (maximum orientation 55°333°),

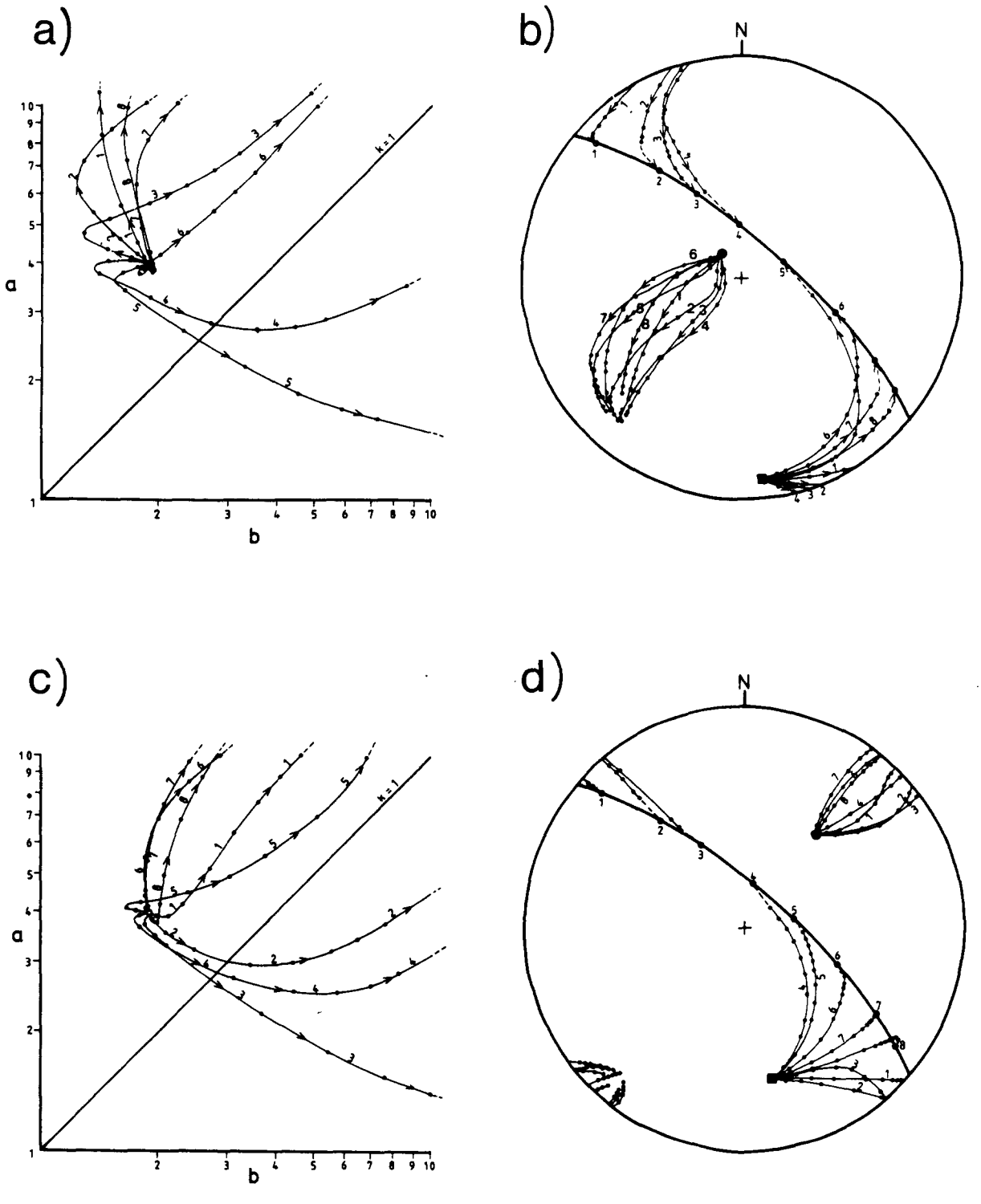

Fig. 10. Irrotational strain model. XY plane of the strain ellipsoid has the orientation 75°040° and the maximum (X) orientations are similar to the eight shear directions listed in Table 1. The strain paths are constructed using the values of plane strain, $a = b = 1.1, 1.25, 1.5, 2.0, 3.0, 4.0, 6.0$ and 8.0. Initial fabrics are as for specimen 1 in the two orientations B and C shown in Fig. 9. (a) and (b) Results for the crest of the fold for strain orientations 1–8. (a) Strain path of principal axis ratios a and b, and (b) strain paths for maximum (X) and minimum (Z). (c) and (d) Results for the southwest limb for strain orientations 1–8. (c) Strain path of principal ratios a and b, and (d) Strain path for maximum (X) and minimum (Z).

and for specimen 5, model 2 (maximum orientation 38°322°) provide the closest fit to the strain data in orientation and fabric type. However, to produce a strain path that completely fits the strain data a more complex model is required.

Comparison of the two models and discussion

Comparison of the two models above shows that:

(1) The rotational strain model provides all fabric types represented by the strain data and field observation whereas the irrotational model requires additional stages to produce the fabrics in the extreme southwest of the Tollie Antiform.

(2) The rotational strain model provides a mechanism for the formation of the Tollie Antiform, whereas the irrotational model does not.

Rotational strain (simple shear) as opposed to irrota-

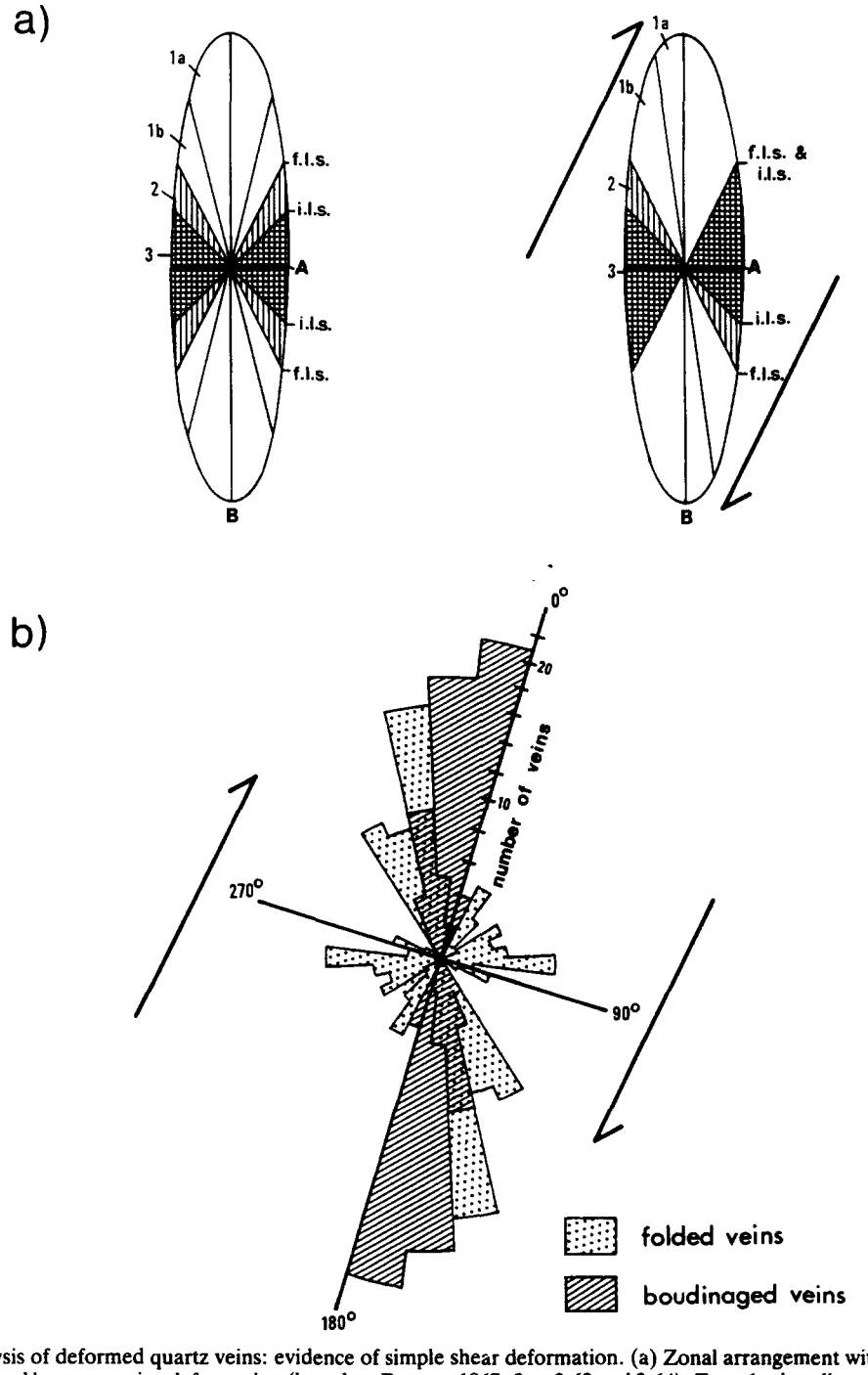

Fig. 11. Analysis of deformed quartz veins: evidence of simple shear deformation. (a) Zonal arrangement within a strain ellipse developed by progressive deformation (based on Ramsay 1967, figs. 3-62 and 3-64). Zone 1a, boudinage only; zone 1b, boudinage in folded bands or boudinaged folds; zone 2, folds being boudinaged; zone 3, folds only. A and B, principal axes of strain; f.l.s., direction of no finite longitudinal strain; i.l.s., direction of no infinite longitudinal strain. (b) Rose diagram of 134 boudinaged and folded quartz vein orientations on sub-horizontal surface. Note large overlap in the region 310–360° and small overlap at around 010° which indicates dextral simple shear in this section.

tional strain (pure shear) is also supported by field evidence.

(1) *Deformed quartz veins.* The relationship between orientations of folded and boudinaged veins is dependent on the type of deformation, i.e. pure or simple shear. In the course of progressive deformation veins can move from the field of contraction to expansion thus causing an overlap in the orientation of folded and boudinaged veins. Zones of overlap are dependent on the type of strain, and are symmetrical in pure shear and asymmetric in simple shear, Ramsay (1967), Fig. 11a.

The orientations of 134 boudinaged and folded veins measured on sub-horizontal erosion surfaces from the southwest limb (Fig. 2), are plotted in Fig. 11(b), and show a strongly asymmetric pattern with a large overlap zone in the region 310–360° and a small overlap around 010°, indicating simple shear as the type of deformation. The foliation in this area trends more northerly than normal for the southwest limb as a whole due to later open folding. Thus the shear trend in Fig. 11(b) is approximately north instead of northwest. Correcting for rotation of foliation the pattern in Fig. 11(b) implies a dextral sense of shear on the horizontal surface which, with the

southwest-side-down sense of shear needed to form the Tollie Antiform, indicates a northwest plunging shear direction in agreement with the conclusions from the strain path modelling.

(2) *Inter-limb angle of folds.* An irrotational strain model will produce progressively tighter folds from northeast to southwest as strain becomes more intense (Fig. 12a). This applies to any pre-existing folds as well as to folds associated with the modelled deformation. In the rotational model, due to the orientation of the northeast limb with respect to the shear plane, original folds will be progressively opened during deformation (Fig. 12b). In the southwest limb where the deformation is strongest, tight shear folds will also develop (Fig. 12b). Only the rotational model, therefore fits the variation in fold interlimb angle observed across the antiform with folds becoming more open from the northeast limb to the crest and progressively tighter across the southwest limb. In the rotational model within the southwest limb the folds developed by shearing have an opposite sense of vergence to those developed by pure shear. Minor folds in the southwest limb become progressively attenuated to the southwest making identification of vergence often impossible. However, in the southwest limb minor folds showing both senses of vergence were observed, reflecting original folds and shear folds whose hinges have rotated towards the shearing direction. Folding in quartz veins in the extreme southwest shows the correct vergence for the rotational (simple shear) model.

Thus both field evidence and theoretical modelling indicate simple shear as the dominant type of deformation. This implies that the Tollie Antiform lies on the northeast margin of a large-scale shear zone. The fabric of the northeast limb is taken as pre-dating the main shear deformation and the model makes no comment on the origin of this fabric. If all fabrics are of simple shear origin a true initial fabric for the northeast limb must be of LS ($K = 1$) type, whereas specimen 1 shows a more linear fabric. Fabrics close to LS exist to the southeast of the sample profile in Fig. 2, represented by specimen A, to which specimen 4 is probably related. To test if this specimen could provide a more primitive initial fabric than specimen 1, the initial fabric of specimen 1 was unsheared, i.e. sheared in a southwest-side-up or positive sense, for the eight shear directions of Table 1, and the results are plotted in Fig. 13. These show that LS ($K = 1$) fabrics of similar orientation to specimen A, but of greater intensity are produced by direction 5 (73°069°). It is possible, therefore, that the variation in strain is due to a change in shearing direction from moderately plunging southeasterly, producing the fabric of specimen A, through a direction down the dip of the shear plane (indicated by unshearing using direction 5 to give the best fit to specimen A), to moderately plunging northwest (indicated by shearing using direction 3 to give best fit to the strain data). Alternatively, specimens A and 1 may represent an original variation in the initial fabric caused by inhomogeneous deformation prior to the northwest shearing event. Further indication of initially variable fabrics is given by the rotational strain model where such variability can explain the wide range of a and b ratios of the strain data. This provides an explanation for the general augen shape of the area of good

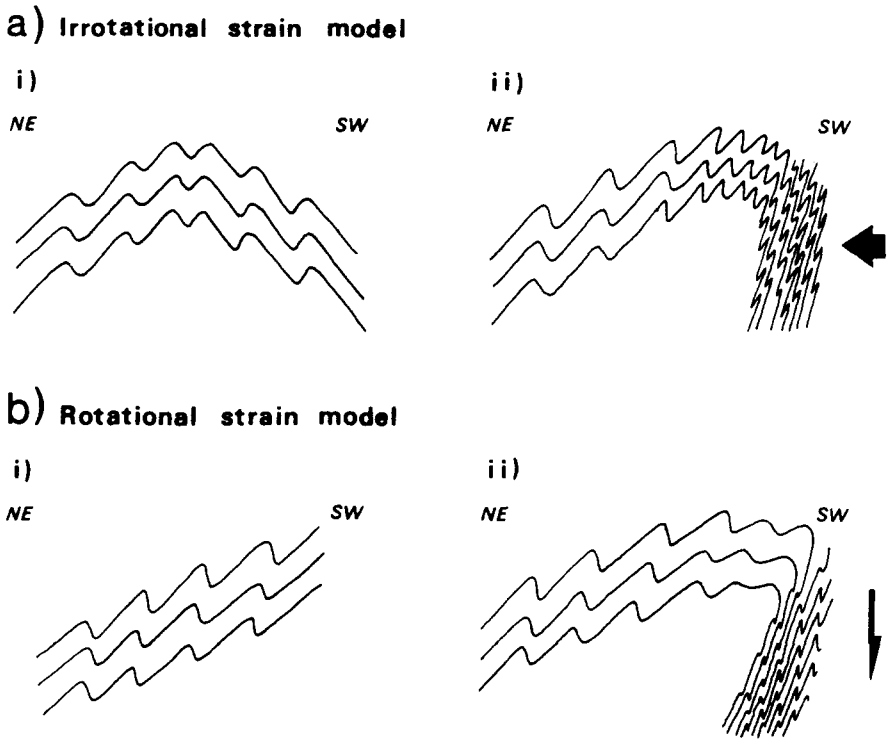

Fig. 12. Schematic vertical cross-sections showing the effect of the strain models on fold interlimb angles. (a) Irrotational strain model: (i) initial concentric fold (Fig. 9) before deformation, (ii) fold after progressive flattening to the southwest. Fold interlimb angles become progressively tighter to the southwest. (b) Rotational strain model: (i) initial state represented by the northeast limb of the Tollie Antiform, (ii) resultant fold after progressive shearing to the southwest. Initial folds of the northeast limb are opened to give large interlimb angles in the crest of the antiform. Shear folds are developed in the southwest limb.

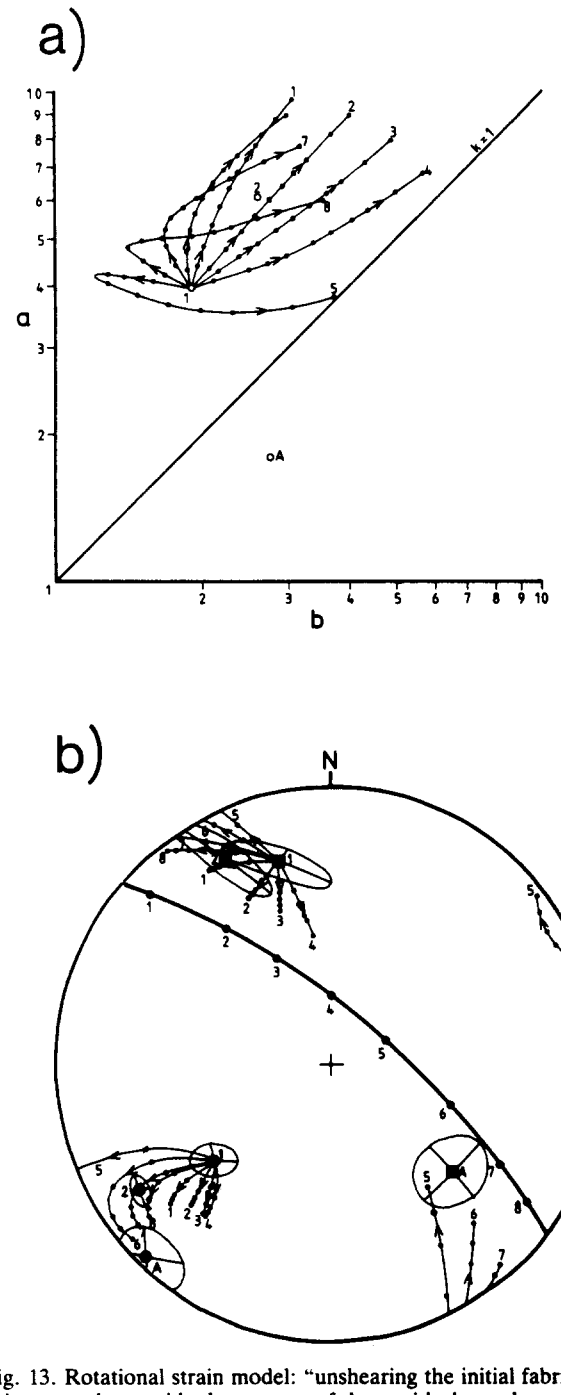

Fig. 13. Rotational strain model: "unshearing the initial fabric", i.e. using a southwest-side-down sense of shear with shear plane orientation, directions 1–8 and strain values as for Fig. 6. 1, specimen 1 from northeast limb (initial fabric); A, specimen A from northeast limb southeast of specimen 1, see Fig. 2. (a) Strain paths for principal axis ratio a (X/Y) and b (Y/Z) for shear directions 1–8. (b) Strain paths for maximum and minimum for shear directions 1–8.

linear fabrics (Fig. 2), as only suitable types of initial fabric would give rise, on subsequent deformation, to good linear fabrics. The true picture may be a combination of these alternatives with specimen 1 incorporating some northwest shear and original variation in initial fabrics causing the limited extent of the development of good linear fabrics.

The probability of variable initial fabrics indicates that the strain analysis and deduced strain path for the deformation apply to the sample profile only. To the south where the Tollie Antiform plunges more steeply southeast, finally becoming north plunging in the extreme southeast of the Lewisian inlier, different attitudes of gneissose layering and initial fabrics will give rise to different sets of finite strain values and strain paths. However, the finite strain results and strain paths presented here, provide a basis for the construction of a strain profile for the area sample and thus, assuming a relatively rigid block to the northeast at the time of shearing, an estimation for the displacement suffered by the Loch Tollie gneisses as a whole.

CONSTRUCTION OF A STRAIN PROFILE

Assuming simple shear, with a shear plane dipping steeply northeast and a shear direction plunging moderately northwest, estimates of the shear strain (γ) have been made for a profile across the Tollie Antiform, by two independent methods: (1) comparing the strain data with rotational strain model 3, and (2) variation in attitude of gneissose layering from northeast to southwest, across the antiform.

(1) *Comparison of the strain data with rotational model 3.* Using the strain paths for model 3 with specimens 1–3 and 5 as initial fabrics, values of shear strain were estimated for each specimen. The strain data form a wide scatter about the ideal paths of specimens 1–3 and 5 shown by model 3. To give an objective estimate of the strain value indicated by models for each data point the following method was applied. Firstly, the position of each specimen with respect to the Tollie Antiform is used to indicate to which portion of the strain path it must be related. Specimens from the hinge zone of the antiform, the northeast, the central and the southwest parts of the southwest limb must relate to the L ($K > 1$), the initial LS ($K \simeq 1$), the S ($K < 1$) and the final LS ($K \simeq 1$) parts of the strain paths, respectively in the direction of increasing strain. For each data point the nearest part of the strain path, such that a perpendicular to the strain path passes through the point, was used as an estimate of the shear strain. If no perpendicular from the appropriate part of the strain path passed through a data point, no estimate of shear strain was made. In this manner a maximum of four estimations of shear strain are obtained from the four strain paths of model 3 using specimens 1–3 and 5 as initial fabrics. The results (Fig. 14) show a gentle increase in strain across the northeast limb and the crest of the antiform with a sharper increase across the southwest limb reaching a value of $\gamma \simeq 6$ at the most southwesterly specimen (specimen 11).

(2) *Variation in attitude of gneissose layering.* Knowing the orientation of the shear plane, direction and sense, shear strain can be estimated by the change in attitude of a plane during progressive deformation using the equation given by Skjernaa (1980, eqn. 2):

$$P' = \tan^{-1}(\tan(P - 90) + \gamma|\cos V|) + 90,$$

where P = initial dip of plane in degrees, P' = final dip of plane in degrees, V = initial strike of plane in degrees.

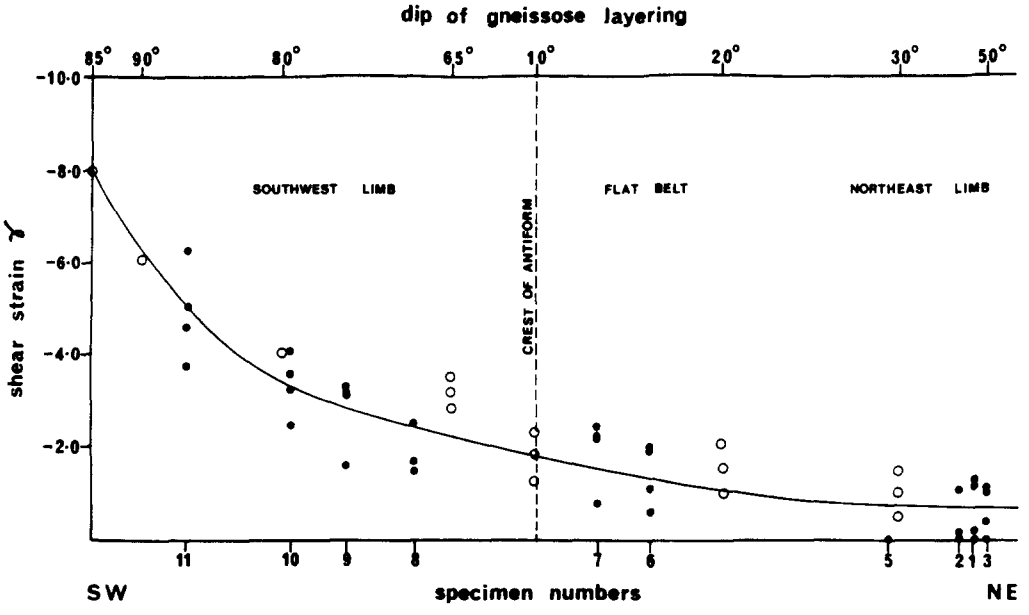

Fig. 14. Strain profile across the Tollie Antiform. Black dots, values of shear strain obtained from comparison of model 3 strain paths and strain data. Open circles, values of shear strain obtained from the attitude of gneissose layering.

The attitude of layering in the northeast limb was taken as the initial orientation and three values of dip, 45, 50 and 55°, with the common direction of dip 052°, were used to represent the variation in initial attitude. For use in the calculation the orientations of initial planes were recalculated relative to a horizontal shear plane and a north trending shear direction, and the results converted back to the geographical reference frame before plotting in Fig. 15. Results of shearing these initial orientations using the shear direction of rotational model 3 are shown in Fig. 15, and show that layering is folded over with progressive deformation to produce an antiform with a hinge plunging respectively 16, 20 and 24° southeast. The trend of the foliation in this southwest limb adjacent to the hinge zone is more northerly than that predicted by the model, due possibly to variations in initial fabric and attitude of gneissose layering. However, the variation in dip of layering can be used to estimate shear strain from the three initial orientations of gneissose layering and the results are plotted, together with the estimates from the strain data, in Fig. 14. As shear strain increases the three models converge on a similar layer orientation for the same shear strain. Thus the results of the three models for the three most southwesterly points on Fig. 14 are represented by one point and the attitude of layering in the extreme southwest of the southwest limb implies a shear strain of $\gamma \simeq 8$. The two sets of data, from comparison of the strain data and rotational model 3 and the variation in attitude of gneissose layering, show close agreement (Fig. 14).

The strain profile in Fig. 14 shows a progressively larger shear strain with increasing gradient to the southwest typical of the strain pattern across the margin of the shear zone. The profile can be used to estimate the displacement across the area by calculating the area under the curve in Fig. 14 as outlined by Ramsay & Graham (1970). This method yields a displacement in the Tollie gneisses of 8.3 km in a southwest-side-down sense and moderately northwest plunging direction, which resolves to 4.7 km horizontal dextral shear and 6.8 km vertical southwest-side-down shear.

CONCLUSIONS AND DISCUSSION

Comparison of present interpretation with previous research

The Loch Tollie gneisses have been analysed structurally by Park (1969). His interpretation divides the deformation into four main phases with a fifth, late stage, brittle phase. Briefly, D1 is the original gneissose layering and D2 comprises isoclinal folds in the northeast limb with associated subvertical, northwest striking foliation. The Tollie Antiform is interpreted as a D3 structure flattened on the southwest limb by D4. Park's D1 and D2 are equivalent to the initial fabric of this interpretation, and his D3 and D4 equivalent to the main shearing event.

Park's D2 with subvertical foliation differs from the initial fabric of the northeast limb which dips more gently northeast. However, as stated above, this initial fabric is likely to have incorporated some of the main shearing deformation, causing a shallowing of the gneissose layering. Specimen 4 from the northeast limb and specimen A from the area 2 km to the south may be more primitive initial fabrics, XY planes dipping steeply northeast in closer agreement with Park's D2 foliation.

Park's model of a D3 fold flattened on the southwest limb by D4 is somewhat similar to the irrotational strain model here, though this model is rejected in favour of the rotational strain model. Thus the lineations in the southwest limb are interpreted by Park as intersection

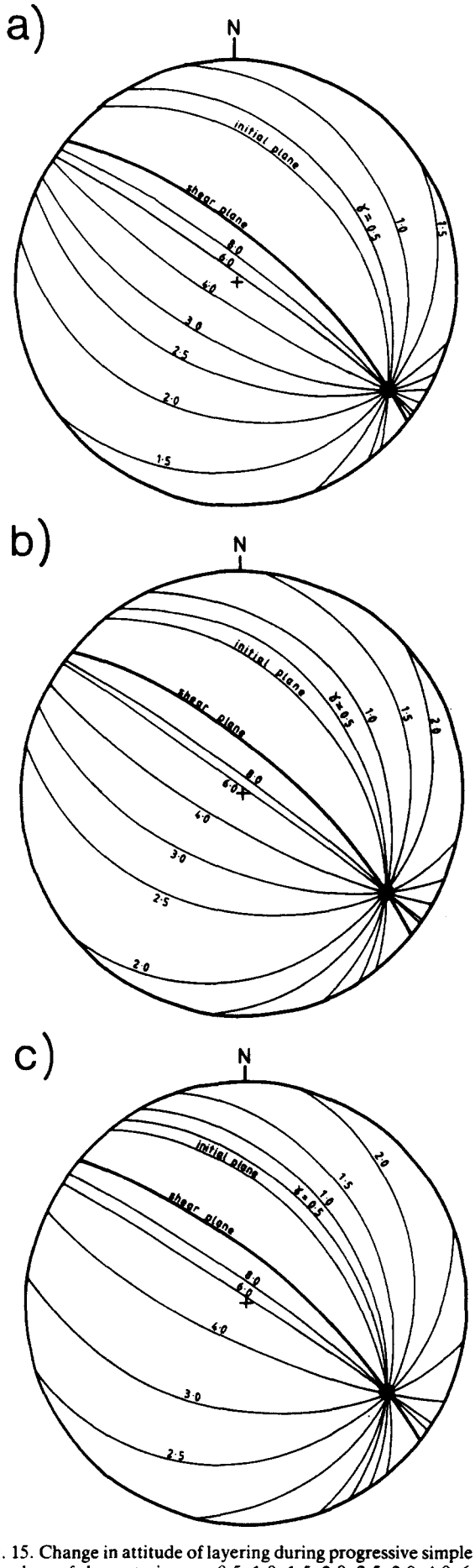

Fig. 15. Change in attitude of layering during progressive simple shear for values of shear strain, $\gamma = 0.5, 1.0, 1.5, 2.0, 2.5, 3.0, 4.0, 6.0$ and 8.0. Shear plane orientation is 75°040° and shear direction is 55°333° (rotational strain model 3). Initial plane orientations are (a) 45°052°, (b) 50°052° and (c) 55°052°. Resulting hinges of folds are (a) 16°126°, (b) 20°125° and (c) 24°122°.

lineations resulting from D3 and D4, whereas here the variation in plunge is interpreted as due to the passive rotation of minor fold hinges which during shearing rotate through horizontal to become northwest plunging (Odling 1980, pp. 79–81).

A gravity survey of the Gairloch area (Fig. 1) has been carried out along two profiles across the Tollie Antiform and the Gairloch schist belt (Thompson & Westbrook 1982). The structural models which fit the gravity data indicate that the Gairloch schists lie in a steep-sided synformal structure extending to depths of between 4 and 6 km. This model differs at depth from the structural model of Park (1964) which predicts the Gairloch schist belt to extend to only approximately 1.5 km depth. The discrepancy is most noticeable at the thick amphibolite sheet on the northeast margin of the schist belt. Park (1964) interprets this amphibolite as lying in the core of a synform extending to approximately 1 km depth whereas the gravity model indicates this amphibolite sheet to extend to depths of between 5 and 6 km. Though it does not exclude the possible presence of large-scale isoclinal folds as proposed by Park (1964), the slab-like geometry of the Gairloch schist belt indicated by the gravity data is also consistent with the shear zone model where the moderately northwest plunging shear direction implies considerable vertical extension.

Significance and extent of the shear zone to the southeast

The Tollie gneisses are interpreted as lying on the northwest margin of a large-scale, northwest trending shear zone that dips steeply northeast and has a southwest-side-down sense of displacement. The foliation in the extreme southwest of the Tollie Antiform, where deformation is strongest and subparallel to layering, can be traced southwestwards through the Gairloch schist belt and approximately 1 km into the South Sithean Mhor gneisses, forming a northwest trending belt some 5 km broad (Fig. 1). This zone therefore represents the zone of strongest shearing deformation.

A northwest plunging shear direction is indicated by lineations and the strain modelling in the Loch Tollie gneisses. However, lineations in the Gairloch schist belt and the South Sithean Mhor gneisses are more variable and form northwest trending belts of alternating northwest and southeast plunging lineations (Park 1964). These are interpreted by Park as due to isoclinal folding of an older lineation. Some of the folds are inferred from the change in plunge of lineations alone whereas other folds, seen to fold the lithological layering, do not fold the lineation. This is explained by Park as two phases of folding, an early phase associated with the lineation (his type I folds) and a later phase folding the lineation (his type II folds). Though it is probable that large-scale isoclinal folds exist in the Gairloch schist belt, an alternative interpretation, favoured here, is that the variation in lineation plunge is due to changes in shear direction throughout the history of the shear zone. Changes in shear direction between northwest and southeast have already been suggested as a possible explanation for the

variation in fabrics on the northeast limb of the Tollie Antiform. Further evidence of a variable shear direction is seen at South Sithean Mhor, immediately to the southwest of the zone of steeply northeast dipping foliation (Odling 1980, pp. 40–41). There, near isotropic shape and mineral fabrics are common in the gneisses and dykes and deformation is characterized by numerous minor shear zones dipping steeply northeast often developed along dyke contacts. Foliation is intense in the centres of these shear zones and the associated lineations are thus assumed to be close to the shear direction. These lineations are highly variable in orientation, both between and within individual shear zones, plunging from 25° northwest to 30° southeast and thus suggesting a variable shear direction.

The schists and amphibolites display signs of extreme deformation, e.g. blastomylonitic textures in the schists, fine grained nature and streaked out feldspar aggregates in the amphibolites, and extreme quartz fabrics developed in the South Sithean Mhor gneisses close to their contact with the schists and in gneiss layers within the schist belt (Odling 1980, chapter 8). Due to a lack of strain markers and the complicated strain history implied by the variation in plunge of lineations, it is not possible to estimate the displacement across the Gairloch schist belt. It is also possible that shear sense as well as shear direction has varied in the schist belt. However, minor features where available within the schist belt, i.e. the rotation of foliation surrounding undeformed pods in the thick amphibolite sheets and indicated by en échelon quartz veins, show a southwest-side-down sense, in agreement with the Tollie Antiform, irrespective of the direction of lineation plunge (Odling 1980, p. 106). From the evidence of extreme deformation and the probability of a constant shear sense, it is likely that the shear displacement in the schist belt far exceeds that in the Tollie gneisses. The estimate of displacement in the Tollie gneisses of 8.3 km, thus provides a minimum value for the displacement of the whole shear zone which is likely to be two or three times that value, i.e. some tens of km.

Age of the shearing event

The age of the deformation can be inferred from a number of age determinations by various workers in the area. Undeformed pegmatites in the crest of the Tollie Antiform are dated at 1720 to 1630 Ma (Holland & Lambert 1973) whereas the age of dyke intrusion is dated at around 2200 and 2100 Ma (Park & Evans 1965, Moorbath & Park 1971). This places the formation of the Tollie Antiform at between 2200 and 1700 Ma, i.e. late Inverian to early Laxfordian according to the chronology of Sutton & Watson (1965). The schists yield younger ages, 1409 ± 35 to 1398 ± 35 (Park & Evans 1965, Moorbath & Park 1971), indicating that deformation continued longer in the schists than in the gneisses. Thus the shear zone was active from the late Inverian or early Laxfordian through to late Laxfordian times.

Relationship of the Gairloch Shear Zone to the rest of the Lewisian complex of NW Scotland

The Lewisian complex of Scotland has been divided by Sutton & Watson (1965) into areas of dominantly Scourian/Inverian deformation and areas of Laxfordian reworking (Fig. 16). The Gairloch Shear Zone lies close to the northern boundary of the southern area of Laxfordian reworking. The Tollie gneisses are bounded to the north by the Loch Maree Fault, north of which the Loch Maree schists and the Gruinard gneisses outcrop. The Loch Maree schists and the Carnmore Antiform in the Gruinard gneisses are correlated with the Gairloch schists and the Tollie Antiform respectively, on the basis of structure and dating (Park 1973, Crane 1978, Bickerman *et al.* 1975). The Gruinard gneisses north of the Carnmore Antiform show low Laxfordian reworking (Davies 1977), and remnant granulite facies assemblages (Field 1978). To the south of the Gairloch Shear Zone lies the Ruadh Meallan belt showing pre-dyke structures and remnant granulite facies assemblages (Cresswell & Park 1973). Southwards from this belt Laxfordian reworking and migmatization become progressively more intense (Cresswell & Park 1973, Sutton & Watson 1965). Thus, in general, the Gairloch Shear Zone acts as a tectonic break between the area of high Laxfordian reworking to the south and the area of low Laxfordian reworking with remnants of Scourian/Inverian structure and mineral assemblages to the north. The sense of

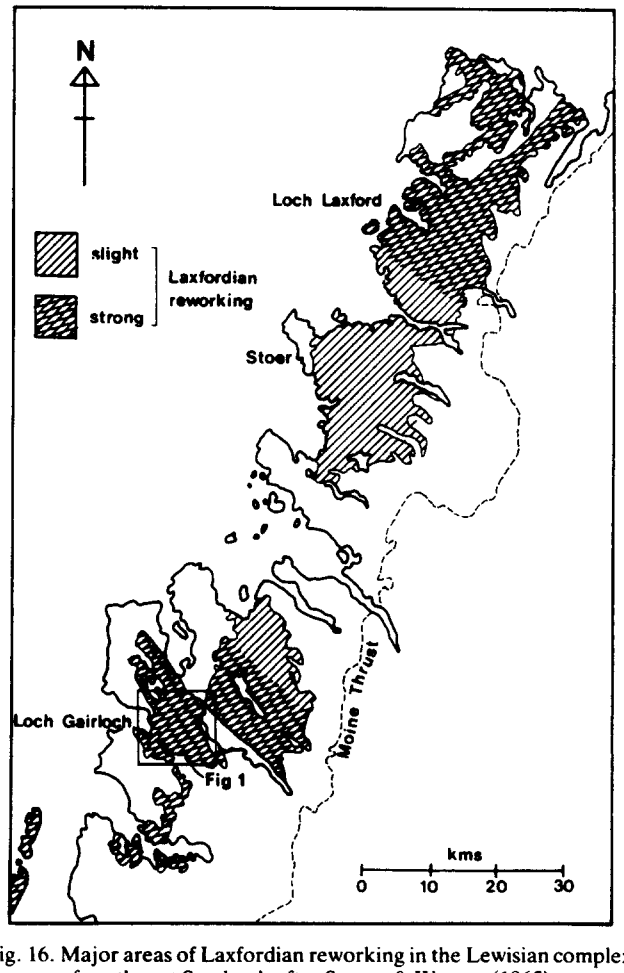

Fig. 16. Major areas of Laxfordian reworking in the Lewisian complex of northwest Scotland, after Sutton & Watson (1965).

shear, southwest-side-down, is consistent with the lower grade of metamorphism (low amphibolite facies) and extensive migmatization of the gneisses to the south, representing a higher structural level than the remnant Scourian/Inverian structure and granulite facies mineral assemblages found in the gneisses to the north. Since the area to the north of the Gairloch Shear Zone is one of low Laxfordian reworking, it formed a relatively rigid block throughout the shearing event. Thus the estimates of displacement from the strain profile presented here (6.8 km vertical and 4.7 km horizontal displacement), also apply to the whole of the Loch Tollie gneisses.

Shear zones of a similar age and sense to the Gairloch Shear Zone, though with a southeast plunging shear direction, have been recorded at Tarbet and Stoer, Sutherland (Beach 1974, Beach *et al.* 1973). The displacement on the Tarbet Shear Zone has been calculated as 18 km in the vertical, and 16 km in the horizontal sense. The estimates here of 6.8 and 4.7 km vertical and horizontal displacement, respectively, for the Tollie gneisses indicates the displacement on the whole of the Gairloch Shear Zone to be of the order of some tens of km. It is probable therefore that the Gairloch and Tarbet Shear Zones have displacements of a similar order of magnitude. An early thrust, now deformed in the Tarbet Shear Zone, has been proposed on the basis of metamorphic, geochemical and geophysical evidence (Beach 1974) to account for the presence of Laxfordian migmatites to the north, i.e. on the upthrow side, of the Tarbet Shear Zone and the shear zone is proposed by Beach (1974) to be a Proterozoic discontinuity of some importance. Thus the Tarbet and associated Stoer Shear Zones, and the Gairloch Shear Zone provide major tectonic discontinuities on the northern and southern margins respectively, of the central mass of Scourian gneisses, separating them from the areas of strong Laxfordian reworking and migmatization.

The shear zone model for the Gairloch area requires a tectonic fabric in the Tollie gneisses, i.e. the fabric of the northeast limb, of early Laxfordian or earlier age, prior to the onset of northwest shearing. Coward (1974) has postulated a major subhorizontal heterogeneous shearing event in early Laxfordian times in which remnants of Scourian structure and mineral assemblages, e.g. the Gruinard gneisses and the Ruadh Meallan belt, are preserved in largely undeformed lenses. This is followed by major upright structures of Laxfordian age of which the Tollie Antiform (and thus the Gairloch Shear Zone), the Carnmore Antiform and the shear zones at Tarbet and Stoer are examples. The early flat-lying Laxfordian shearing event is a possible origin for the initial fabric of the northeast limb of the Tollie Antiform. As the early deformation proposed by Coward (1974) is by shearing (simple shear) the associated fabrics will approximate to LS in type. Close to LS fabrics are found in the northeast limb, specimen 4, and to the south of the sample profile, specimen A. These fabrics are not flat-lying but their location on the edge of a relatively undeformed lens, the Gruinard gneisses, may account for their steep attitude. The heterogeneous nature of this early event is consistent with the lensoid nature of the area of linear fabric in the crest of the Tollie Antiform and the wide range of a and b ratios of the finite strain results.

Acknowledgements—The research presented in this paper was carried out during tenure of a part-time demonstratorship in the Department of Geology, Queen's University of Belfast, Northern Ireland, while the author was registered as a post-graduate student at Edinburgh University. Many thanks go to Dr. R. F. Cheeney (Edinburgh) for supervising the research and to Dr. A. Beach (Liverpool) and Dr. D. Sanderson (Belfast) for their kind help and advice. An earlier version of this article has been substantially improved in the light of comments and suggestions by two anonymous referees.

REFERENCES

Bailey, E. H. & Stevens, R. E. 1960. Selective staining of K-feldspar and plagioclase on rock slabs. *Am. Miner.* **45**, 1020–1025.

Beach, A. 1974. The measurement and significance of displacements on Laxfordian shear zones, N.W. Scotland. *Proc. geol. Ass.* **85**, 13–21.

Beach, A., Coward, M. P. & Graham, R. H. 1973. An interpretation of the structural evolution of the Laxford front, north-west Scotland. *Scott. J. Geol.* **9**, 297–308.

Bickerman, M., Bowes, D. R. & Van Breemen, O. 1975. Rb–Sr whole rock isotopic studies of Lewisian metasediments and gneisses in the Loch Maree region, Ross-shire. *Q. Jl geol. Soc. Lond.* **131**, 237–254.

Coward, M. P. 1974. Flat-lying structures within the Lewisian basement gneiss complex of N.W. Scotland. *Proc. geol. Ass.* **85**, 459–472.

Crane, A. 1978. Correlation of metamorphic fabrics and the age of the Lewisian metasediments near Loch Maree. *Scott. J. Geol.* **14**, 225–246.

Creswell, D. & Park, R. G. 1973. The metamorphic history of the Lewisian rocks of the Torridon area in relation to that of the remainder of the southern Laxfordian belt. In: *The Early Precambrian of Scotland and Related Rocks of Greenland.* (edited by Park, R. G. & Tarney, J.). University of Keele, 77–84.

Davies, F. B. 1977. The Archean evolution of the Lewisian complex of Gruinard bay. *Scott. J. Geol.* **13**, 189–196.

Dunnet, D. 1969. A technique of finite strain analysis using elliptical particles. *Tectonophysics* **7**, 117–136.

Dunnet, D. & Siddans, A. W. B. 1971. Non-random sedimentary fabrics and their modification by strain. *Tectonophysics* **12**, 307–325.

Field, D. 1978. Granulites at Gruinard bay. *Scott. J. Geol.* **14**, 359–361.

Hext, G. R. 1963. The estimation of the second-order tensors with related tests and designs. *Biometrika* **50**, 353–372.

Holland, J. G. & Lambert, R. St. J. 1973. Comparative major element geochemistry of the Lewisian of mainland Scotland. In: *The Early Precambrian of Scotland and Related Rocks of Greenland.* (edited by Park, R. G. & Tarney, J.). University of Keele, 51–62.

Moorbath, S. & Park, R. G. 1971. The Lewisian chronology of the southern region of the Scottish mainland. *Scott. J. Geol.* **8**, 51–74.

Odling, N. E. 1980. Structural, textural and metamorphic studies in the Lewisian of Gairloch, N.W. Scotland. Unpublished Ph.D thesis, University of Edinburgh.

Park, R. G. 1964. The structural history of the Lewisian rocks of Gairloch, Wester Ross, Scotland. *Q. Jl geol. Soc. Lond.* **120**, 397–433.

Park, R. G. 1969. The structural evolution of the Tollie Antiform—a geometrically complex fold in the Lewisian northeast of Gairloch, Ross-shire. *Q. Jl geol. Soc. Lond.* **125**, 319–349.

Park, R. G. 1973. The Laxfordian belts of the Scottish mainland. In: *The Early Precambrian of Scotland and Related Rocks of Greenland.* (edited by Park, R. G. & Tarney, J.). University of Keele, 65–76.

Park, R. G. & Evans, C. R. 1965. K–Ar age determinations from the Lewisian of Gairloch, Ross-shire, Scotland. *Nature, Lond.* **205**, 350–352.

Peach, B. N., Horne, J., Gunn, W., Clough, C. T. & Hinxman, L. W. 1907. The geological structure of the north-west highlands of Scotland. *Mem. Geol. Surv. G.B.*

Ramsay, J. G. 1967. *The Folding and Fracturing of Rocks.* McGraw-Hill, New York.

Ramsay, J. G. & Graham, R. H. 1970. Strain variations in shear belts. *Can. J. Earth Sci.* **7**, 786–813.

Sanderson, D. J. 1976. The superposition of compaction and plane strain. *Tectonophysics* **30**, 35–54.

Shimamoto, T. & Ikeda, Y. 1976. A simple algebraic method for strain estimation from deformed ellipsoidal objects—I. Basic theory. *Tectonophysics* **36**, 315–337.

Skjernaa, L. 1980. Rotation and deformation of randomly oriented planar and linear structures in progressive simple shear. *J. Struct. Geol.* **2**, 101–109.

Sutton, J. & Watson, J. 1965. Scourian-Laxfordian relationships of northwest Scotland. In: *The Archean.* (edited by McCall, J.). Dowden, Hutchison & Ross, Stroudsburg, Pennsylvania, 284–293.

Thompson, M. W. H. & Westbrook, G. K. 1982. A gravity investigation of the deep structure of the Lewisian rocks of Gairloch, Wester Ross. *Scott. J. Geol.* **18**, 177–185.

Topping, J. 1958. *Errors of Observation and their Treatment.* Chapman and Hall, London.